International Journal of Applied Earth Observation and Geoinformation 64 (2018) 301–310

Contents lists available at ScienceDirect

International Journal of Applied Earth Observation and Geoinformation

journal homepage: www.elsevier.com/locate/jag

Application of visible and infrared spectroscopy for the evaluation of evolved glauconite

Shovan L. Chattoraj [a,*], Santanu Banerjee [b], Freek van der Meer [c], P.K. Champati Ray [a]

[a] Indian Institute of Remote Sensing,Indian Space Research Organization, 4-Kalidas Road, Dehradun 248001, India
[b] Department of Earth Sciences, Indian Institute of Technology Bombay, Powai, Mumbai 400076, India
[c] Department of Earth Systems Analysis, University of Twente, Faculty of Geo-Information Science and Earth Observation (ITC), The Netherlands

ARTICLE INFO

Article history:
Received 6 August 2016
Received in revised form 31 January 2017
Accepted 6 February 2017
Available online 23 February 2017

Keywords:
Glauconite maturity
Visible-SWIR
Expandable layers
Reflectance
Emissivity

ABSTRACT

The Oligocene Maniyara Fort Formation in western India exhibits two distinct glauconite types with different maturation states, which are characterized by their spectral response in the visible to infrared spectrum of electromagnetic radiation. Spectral signatures of Maniyara Fort glauconites display absorption features at approximately 0.77, 1.08, 1.9, 2.3 μm in the visible-short-wave infrared (SWIR) and 2.8 and 10 μm in the mid-infrared (MIR) region which vary with K_2O content of glauconite. The spectra of glauconite varies significantly as a function of its cationic contents and substitution in different sites. The maturity is found to increase in tandem with the metal–metal charge transfer (CT) and the Fe^{2+} dd absorption band respectively at 1.08 and 0.77 μm. H_2O and OH^- signatures at the NIR region reflect differences in the sensitivity of glauconites with different molecular H_2O content. In the MIR region, a gradual shift of the Si—O stretch at 10 μm towards lower wavelengths indicates the dominance of smectite layers in glauconites. This study demonstrates a strong correlation between the proportion of expandable layers in the glauconite structure with variations in characteristic band position, depth and symmetry in reflectance and emissivity.

1. Introduction

Glauconite mostly occurs as pellets of 50–1000 μm in diameter and it consists of dioctahedral sheet silicates similar to biotite in terms of structure, but compositionally akin to muscovite (Deer et al., 2013; Jarrar et al., 2000; Odin and Matter, 1981). Glauconitic smectite and glauconitic mica are the two end members of glauconitic minerals, the proportion of expandable layer contents dominates the former (Odin and Matter, 1981). The origin of glauconite is explained by two popular hypotheses. The 'verdissement theory' considers initial precipitation of glauconitic smectite within pores of bioclasts and faecal pellets, which subsequently matures into glauconitic mica by the addition of K_2O at a constant $Fe_2O_{3(total)}$ (Odin and Matter, 1981). The 'layer lattice theory', on the other hand, considers the formation of glauconite from degraded layer silicates, which involves the simultaneous increase of both K_2O and $Fe_2O_{3(total)}$ (Burst, 1958a,b). On the basis of K_2O content glauconite may be classified into four types, i.e. nascent (2–4%), slightly evolved (4–6%), evolved (6–8%) and highly evolved (>8%) (Amorosi, 1995, 1997; Odin and Matter, 1981). As the state of maturation of glauconite depends on the sedimentation rate, a highly evolved glauconite (>8% K_2O) indicates significant stratigraphic condensation (Amorosi, 1995; Banerjee et al., 2016a,b, 2015; Odin and Fullagar, 1988; Odin and Matter, 1981). The origin of K-rich glauconite is related to its higher degree of maturation (Amorosi et al., 2007; Odin and Matter, 1981). Additionally, evolved glauconites are considered as important datable material in a sedimentary sequence (Odin and Fullagar, 1988; Stille and Clauer, 1994).

The spectral properties of phyllosilicate minerals in the 0.4–2.5 μm region have been studied extensively because the diagnostic absorptions can provide crucial information on the chemical composition and crystal structure (Bishop et al., 2002, 2008; Clark, 1983, 1999; Post and Noble, 1993).

Various investigators have investigated the qualitative and quantitative relationships between the structure of a clay/mica group of minerals and the number, depth and position of absorptions employing both visible and infra-red spectroscopy (Aines and Rossman, 1984; Besson and Drits, 1997; Bishop et al., 2002, 2008; Buckley et al., 1978; Crowley and Vergo, 1988; Hunt and Turner, 1953; Nahin, 1955; Rossman, 1988a). While the absorptions due to

* Corresponding author.
E-mail addresses: shovan.iitb@gmail.com (S.L. Chattoraj), santanu@iitb.ac.in (S. Banerjee), f.d.vandermeer@utwente.nl (F. van der Meer), champati_ray@iirs.gov.in (P.K. Champati Ray).

http://dx.doi.org/10.1016/j.jag.2017.02.007
0303-2434/

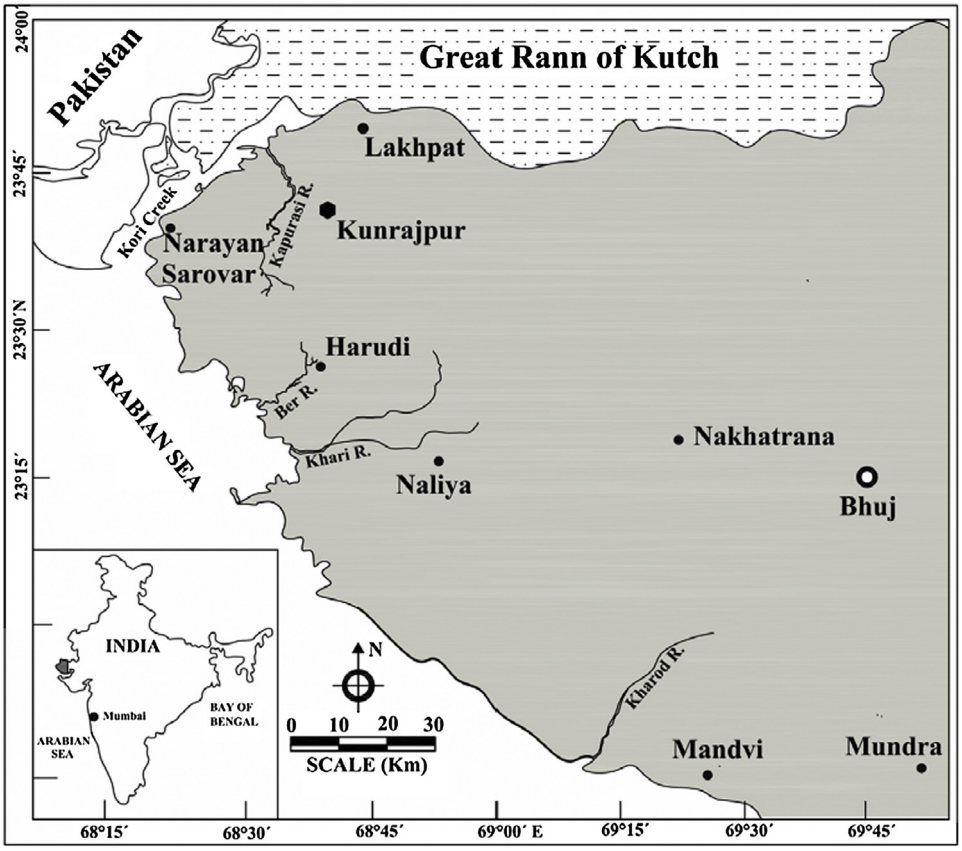

Fig 1. Location map of the study area showing the western part of the Kutch District, India (Grey shaded area in inset shows the same).

OH-stretching of clay/mica group of minerals have drawn attention over decades, characteristic absorptions due to presence of combinations of H—O—H bend, metal (Al, Mg)—OH bend in addition to OH stretch in the VIS-NIR region have also been studied (Burns, 1993; Clark et al., 1990; Mitra, 1996; Slonimskaya et al., 1986; Petit et al., 1998, 1999; Rossman, 1988b). Optical spectroscopy, additionally, enables determination of the presence of Fe^{2+} and Fe^{3+}, both of which are octahedrally coordinated in mica group of minerals like glauconite.

To date few studies report on the maturity of glauconites and its possible imprints on spectral signatures. Manghnani and Hower (1964a,b) reported Si—O absorptions in the mid infrared region and related to expandable layers in gluaconite and tetrahedral ionic substitution and charge. Sanchez-Navas et al. (2008) correlated colour of glauconites as a maturation indicator and calibrated spectral absorption features due to presence of H_2O at different bands in the VIS-NIR range with maturity. Lyon and Tuddenham (1960) linked the shape of absorption spectra of mica in the 9–10 μm region to the amount of aluminum substitution in the silicon tetrahedral site. Pertinently, glauconitic minerals have ubiquitously been reported from all formations of the Palaeogene succession of Kutch (Chattoraj et al., 2008a,b, 2009; Chattoraj, 2011, 2016; Biswas, 1992; Singh, 1978) which is the focus of the study. Chattoraj (2011) studied stratigraphic implications of the glauconite rich green shales from the Kunrajpur area and presented a detailed geochemical database of the glauconites. However, there is no previous work reported on the identification and characterization of the maturation state of these otherwise well illustrated glauconites using spectroscopic methods. This study envisages the spectroscopic characterization of the Maniyara Fort glauconites, of the Kutch district in India, for understanding glauconite maturation and explores the relationship between geochemical characteristics and the spectral response of glauconite. Banerjee et al. (2012a) presented a geological and geochemical database of the glauconites as well as stratigraphic implications of Maniyara Fort glauconites. The central theme of the present investigation involves recognition of spectral signatures of different types of glauconites approximately at 0.7, 1.08, 1.9, 2.3 μm in the Visible-SWIR and 2.8 and 10 μm in the IR region. Further, the paper presents a variation of spectral characteristics in response to the presence of 1) octahedral Fe^{2+}, Mg^{2+} and Al^{3+}, 2) tetrahedral Al^{3+} and Si^{4+}, 3) molecular H_2O and 4) associated smectitic expandable layer.

Table 1
Oligocene stratigraphy and lithological variations in Maniyara Fort Formation (after Biswas, 1992).

Age	Formation	Member	Lithology
Neogene Formations			
Oligocene	Maniyara Fort	Bermoti	Foraminiferal limestone
		Coral limestone	Foraminiferal and Coralline limestone
		Lumpy Clay	Grey shale
		Basal Member	Green, red shale and limestone
Paleocene to Eocene Formations resting on Deccan Basalt basement			

2. Geological background

One of the major glauconitic intervals in the Paleogene (~65–23 My) of the Kutch district was investigated around the Kunrajpur village (Fig. 1; Table 1 Banerjee et al., 2012a,b; Biswas, 1992; Chattoraj et al., 2008a; Burns, 1993; Clark et al., 1990; Mitra, 1996). The study area near Kunrajpur (23°43′28.80″N, 68°43′ 43.20″E) exposes two Palaeogene formations, viz., the Fulra Limestone (av.

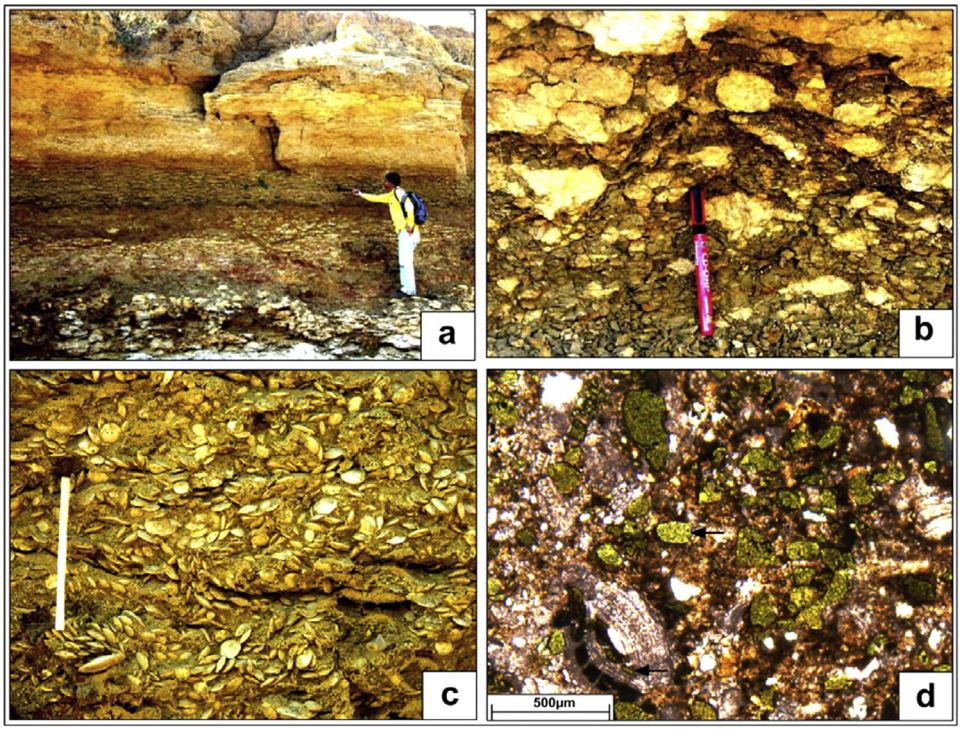

Fig. 2. Field and photomicrograph of glauconite: (a) Field photograph of the sample location showing green and grey shale in section (green shale has been pointed). (b) Close up of the green shale facies rich in glauconite (Pen length = 10 cm). (c) Close up view of the grey shale facies rich in fossils of foraminifera (length of matchstick = 40 mm). (d) Thin section of the green shale facies in crossed polarized light showing glauconite occurring as pellets and few infillings within foraminifera shell (black arrows). (For interpretation of the references to colour in this figure legend, the reader is referred to the web version of this article.)

thickness 80 m) and the Maniyara Fort Formation (av. thickness 20 m). The present work focuses on the Maniyara Fort Formation, which consists of red, grey and green shales and fossiliferous limestones (Fig. 2a–c). It consists of three members, including the Basal, Coral Limestone and Bermoti (Table 1). Bio-stratigraphic analysis of the foraminifera provides an age viz. 35–29 My for Basal and Coral Limestone and an age of 29–23 My for the Bermoti Member (Raju, 1974; Saraswati, 1995). The glauconitic layer of the Maniyara Fort Formation occurs within the Basal Member.

3. Materials and methods

Fifteen spot samples were collected in the field from the green shale, grey shale and limestone facies of the basal member for carrying out geochemical and spectroscopic analysis of glauconite. The glauconite pellets were manually picked using a Nikon SMZ645 stereo zoom microscope and disaggregated samples to maintain its purity. Samples were powdered to a −200 ASTM mesh size (grain size <0.074 mm). The clay fractions were separated by settling method (6 h in distill water). Spectra from dry samples were collected using an Analytical System Device (ASD) fieldSpec4 in the wavelength range of 0.35–2.5 and 1–2.5 μm, at a sampling interval of 1.4 nm and 2 nm respectively. A contact probe was used to nullify the effect of the atmosphere.

The infra-red spectrometer used in this work was a Designs & Prototypes micro-FTIR (Fourier transform infrared spectrometer) Model No. 102F that mimics the design of a Michelson interferometer with an input foreoptic, an infrared detector, drive and sampling electronics and an embedded computer. The instrument has a spectral range of 2–16 μm. It has a rotatable foreoptic with a diameter of about 1 inch and a 4.8° field of view. A digital inclinometer was used to set the foreoptic at a 45° off-nadir viewing angle resulting in a spot size of roughly 3 in. in diameter on a target with a 1 m target distance. The device contains a software package viz. Win FTTM (Version. 1.1.7 on Windows OS) that allows the user to collect real time radiance data to facilitate post processing retrieval of emissivity spectra. Computation of each target emissivity spectra needs four radiance measurements consisting of a cold and warm blackbody, the target and the downwelling radiance. If the atmospheric and background noises are eliminated, spectral emissivity of the target can be calculated from three components viz. the surface-leaving radiance from the target of interest, the downwelling radiance and the surface temperature.

An electronic blackbody with an adjustable temperature has been supplied with the instrument. In general, the cold blackbody temperature is typically set at 10 °C below that of the sample and conversely, the warm blackbody temperature is set just above the warmest object expected (Archer et al., 2015). In this work, these were respectively set to 10 °C and 50 °C to embrace the whole range of temperatures for all samples during data collection in the field. The blackbody calibration was performed with every alternate sample measured or in every 10 min. This minimized sensor drift effects on measurements due to temperature changes.

Downwelling radiance was measured immediately following the sample by collecting the reflected radiance off a diffuse reflective gold plate. InfraGold, supplied by Labsphere, USA served as the standard gold plate in this case. This was placed in the same orientation and position as the target. The gold plate exhibits a relatively flat spectral behavior across the 3–5 μm and 8–14 μm windows with a reflectivity between 0.94 and 0.96. The extremely low emissivity and relatively high thermal mass resulted in accurate downwelling radiance retrieval.

Emissivity of the sample was measured with Hanning apodization to reduce leakage in discrete Fourier transforms. The number of coadds i.e. density of scan lines were fixed at 80 for collecting the spectra (see Salvaggio and Miller, 2001). The temperature of the samples were measured using a handheld Exergen Precision Infrared Handheld Thermometer (DX series), which uses a detector

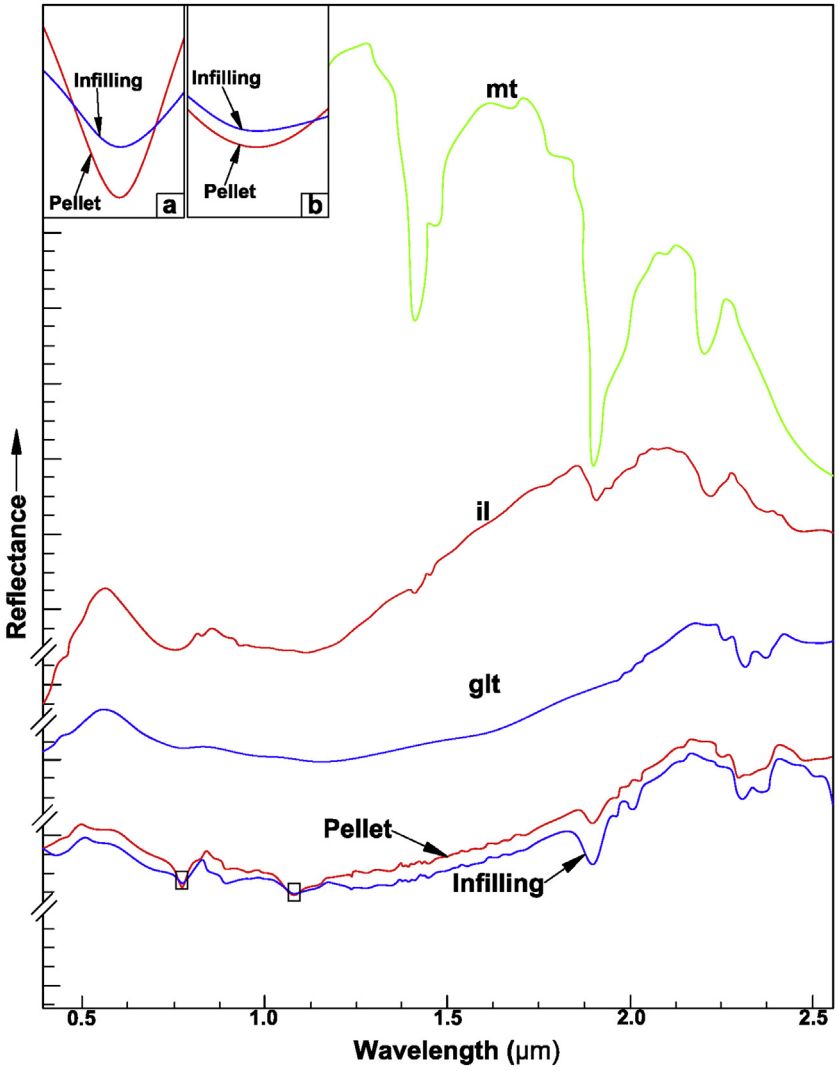

Fig. 3. Reflectance spectra of USGS standard minerals viz. montmorillonite (montmor6.spc Montmorillonite CM 20), illite (illite2.spc Illite IMt-1.a) and glauconite (glauconi.spc Glauconite HS313.3B) available in usgs_min.sli library (ENVI, Ver. 5) and studied glauconite infilling and pellets in the 0.5–2.5 μm range (Abbreviations used for standards: mt – Montmorillonite, il – Illite, glt – Glauconite) [Inset: Enlarged view of the selected portions of the spectra of studied glauconite showing difference in depth of absorption between pellet and infillings at 0.77 μm (a) and 1.08 μm (b)] (Spectral offset given for clarity).

housed inside a contact probe. Subsequently, temperature emissivity separation (TES) data processing was applied to raw radiance data using a series of Interactive Data Language (IDL) codes. First the raw values obtained from the sample and the downwelling measurement were converted to calibrated spectral radiance with the help of the blackbody curves. If the temperature, T_{samp} is known, the emissivity of the sample, ε_{samp} can be derived by:

$$\varepsilon_{samp} = (L_{samp} - L_{dwr})/[L_{BB}(T_{samp}) - L_{dwr}]$$

where, L_{samp} is the measured spectral radiance from the sample, L_{dwr} is the measured reflected downwelling spectral radiance, and L_{BB} (T_{samp}) is the computed blackbody radiance at the sample temperature. As the FTIR rests as close as 1 m from the sample, path radiance and transmission were expected to be 0 and 1 respectively, thereby assuming that the sensor reaching radiance was equal to the surface exiting radiance.

To reduce atmospheric noise, the month of December was preferred for collection of field spectra when the environment is relatively drier. The contribution of reflected and emitted radiance from background objects were eliminated by collecting the spectra in an open free space. The field spectrometer was set up in a way that the direct sunlight falling on the sample was unobstructed. If the sun was in the southern sky, the foreoptic of the instrument was made to lie to the South side of the instrument with the operator to the North side. Downwelling Measurements were carried out in the late afternoon to avoid the rising thermal currents at the hottest point of the day which could contribute to instability in the downwelling radiance field.

The spectral reflectance of rocks were compared with that of the USGS mineral spectral library available in the range of 0.39–2.56 μm in the ENVI 5 software using the spectral library viewer. The spectral analysis tool was utilized for this purpose. A minimum mutual similarity of 85% was considered as significant, beyond which a spectral mismatch was observed. The absorption-band parameters were calculated on the basis of standard procedures (see Clark et al., 1987; Green and Craig, 1985; Kruse et al., 1985; van der Meer, 2004; Yamaguchi and Lyon, 1986). An absorption-band position is the exact reflectance minima in the wavelength region of interest. The absorption-band depth, synonymous with band depth, approximates the reflectance value at the shoulders minus the reflectance value at the absorption-band minimum. The absorption-band asymmetry measures the ratio between the area available at the left and right of the absorption

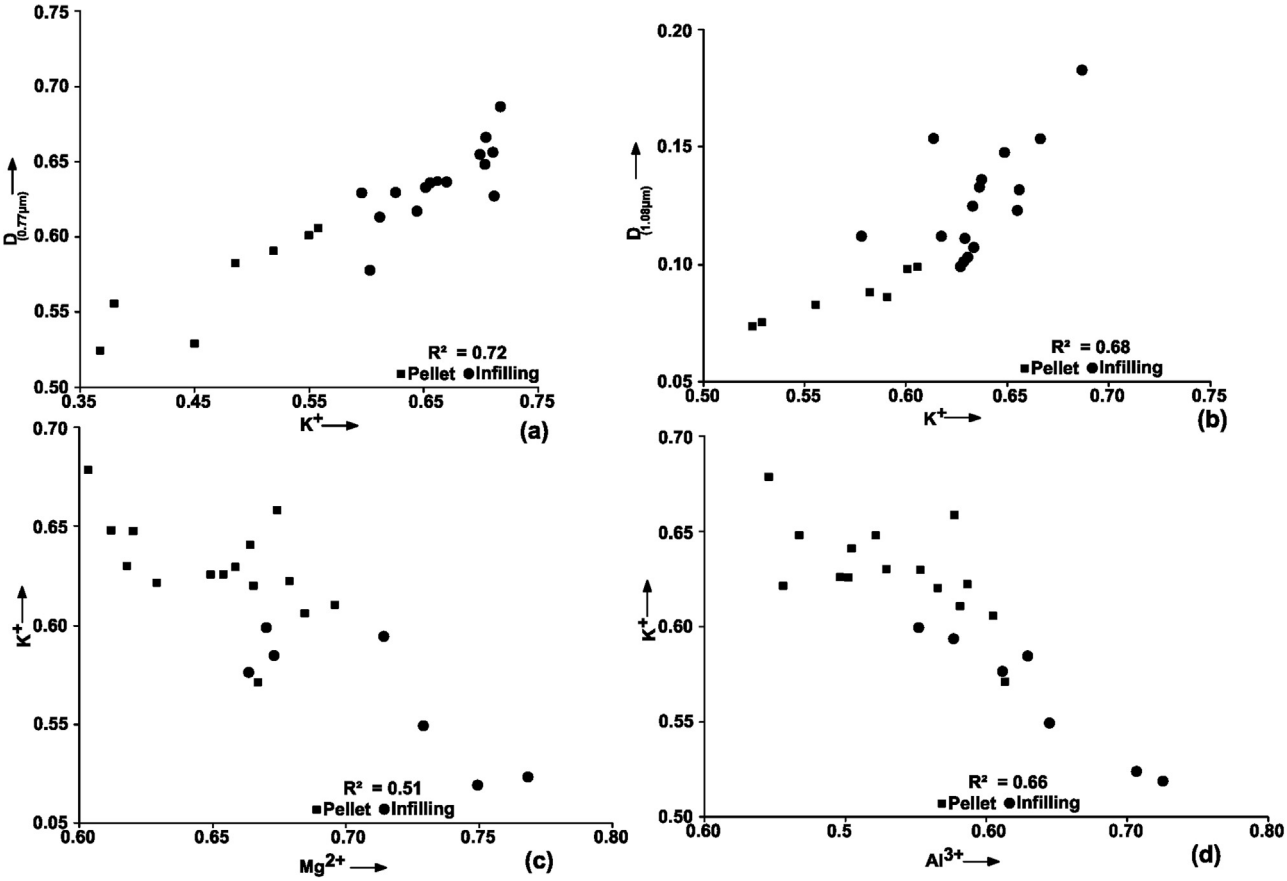

Fig. 4. Cross plots showing the variation in K^+ content of glauconitic pellets and infillings with absorption depths and other cations: (a) 0.77 μm represents a strong positive correlation; (b) 1.08 μm represents a moderate positive correlation; (c) moderate to strong negative correlation between Al^{3+} and K^+ content; and (d) Mg^{2+} with respect to K^+ content suggests a gradual decrease of Mg^{2+} with increasing maturity.

minima i.e. from the respective shoulders on both sides of the maximum absorption.

4. Physical and geochemical description of glauconite

Chattoraj (2011, 2016) and Banerjee et al. (2012b) provided geochemical data for the Maniyara Fort glauconites. Glauconite occurs in two different forms, viz. pellets and infillings. While pellets occur as separate grains, infilling is found within fossilized foraminiferal chambers (Fig. 2d). Glauconitic pellets appear as dark green whereas infillings appear as brownish green under cross polars.

Mineral chemical investigation reveals slightly higher K_2O (av. 6.8 wt%) in pellets than the infillings (av. 6.1 wt%) from EPMA analysis. The infillings provide an asymmetrical, relatively flat basal (001) XRD reflection at 10 Å, while pellets exhibit sharp and symmetrical basal reflection. Glauconite infillings are, therefore, less mature than glauconite pellets and contain more expandable layers. The $Fe^{3+}{}_t$ content of glauconite pellets is higher (av. 26.6 wt%) compared to that of glauconite infillings (av. 24.8 wt%). MgO and CaO values are slightly lower in glauconite pellets compared to the glauconite infillings. The overall high Mg and low Al contents distinguish Maniyara Fort glauconites from other glauconites of the Kutch district (Banerjee et al., 2012a; Chattoraj, 2011, 2016). The cationic contents of both varieties of glauconites and their site charges were calculated and are shown in Table. 2. The cation content of glauconite samples are compared with the corresponding spectral response as spectral characteristics are more closely related to cations present in the crystal lattice than abundance of major oxides. All elemental determinations were made on an anion equivalent basis to structural formulae per $O_{10}(OH)_2$.

Maturation of both glauconite infillings and pellets took place with the synchronous addition of Fe in octahedral sites and fixation of K in the interlayer sites, while Al, Mg and Ca were released concomitantly from the substrate. A model combining initial authigenic precipitation of glauconitic smectite, followed by incorporation of both Fe and K during later stages of maturation explains the origin of glauconite (Banerjee et al., 2012b; Chattoraj, 2011, 2016). The significantly high Mg content of the glauconites relates to Mg-rich smectitic substrates, which is enriched in expandable layers. Nd concentrations of glauconite pellets in the Maniyara Fort Formation suggest a low to moderate sediment accumulation rate (Banerjee et al., 2012b).

5. Results and interpretations

5.1. Spectral signatures in VIS-NIR range

The pellets exhibit intense, sharp and symmetric 0.770 and 1.080 μm absorptions (Fig. 3). These pellets contain more Fe^{3+} (av. 1.52) compared to infillings (av. 1.40) (Table 2). K^+ content of all pellets and infillings exhibits a good correlation with the depth at 0.77 μm and 1.08 μm (Fig. 4a–b). Extrapolation of linear regression equation of this trend provides the K^+ content of glauconites.

Both metal–metal Charge Transfer (0.77um) and Fe2+ *dd* absorption (1.08 μm) depth increase with maturity of glauconites. The effect of CT appears to be more intense (higher absorption) in pellets than infillings (Fig. 3). Interestingly, their ratio i.e. D

Table 2
Cationic contents (calculated from major oxide wt% derived from EPMA) of glauconite pellets and infillings showing major cations distribution in different sites, tetrahedral, octahedral charges and absorption depths, wavelengths and ratios related to characteristic absorptions in VIS-NIR to mid infrared range of spectra. (Note: Al^{3+} includes both octahedral and tetrahedral occupancy; Total Fe is represented by $Fe^{3+}{}_t$) (Abbreviation used: D-Depth, E-Emissivity, λ – Wavelength of Emissivity minima, P- Pellet and I- Infilling samples)

Sample No.	Geochemical Parameters										Spectroscopic parameters					
	Tetra and Octahedral Cations					Interlayer Cations			Tetrahedral Charge	Octrahedral Charge	Visible to Short Wave Infra Red			Near to Mid Infra Red		
	Si^{4+}	Al^{3+}	Fe^{3+}	Mg^{2+}	Mn^{2+}	Ca^{2+}	K^+	Na^+			$D_{0.77\ \mu m\ ab.}$	$D_{1.08\ \mu mab.}$	Ratio $D_{(1.08/0.77)}$	$D_{2.2\ \mu m}$	$D_{2.8\ \mu m\ (E)}$	$\lambda_{Si-O\ strech}$
40/1-P	3.50	0.58	1.50	0.68	0.00	0.02	0.67	0.01	0.50	0.43	0.704	0.154	0.219	0.258	0.990	10.15
48/1-P	3.59	0.53	1.48	0.63	0.00	0.03	0.65	0.02	0.41	0.39	0.699	0.123	0.176	0.211	1.128	10.32
54/1-P	3.56	0.46	1.59	0.64	0.00	0.03	0.63	0.02	0.44	0.39	0.596	0.111	0.186	0.156	1.128	10.14
58/1-P	3.50	0.59	1.50	0.69	0.00	0.04	0.63	0.01	0.50	0.43	0.625	0.103	0.165	0.260	1.115	10.11
60/1-P	3.53	0.59	1.45	0.70	0.00	0.03	0.62	0.01	0.47	0.45	0.644	0.112	0.174	0.275	1.223	10.11
61/1-P	3.55	0.51	1.54	0.66	0.00	0.04	0.63	0.01	0.45	0.42	0.655	0.108	0.165	0.223	1.080	10.15
62/1-P	3.53	0.51	1.55	0.67	0.00	0.04	0.65	0.01	0.47	0.42	0.704	0.148	0.210	0.268	1.200	10.20
63/1-P	3.58	0.45	1.57	0.61	0.00	0.03	0.69	0.01	0.42	0.38	0.717	0.183	0.255	0.083	0.802	10.44
66/1-P	3.57	0.50	1.52	0.66	0.00	0.04	0.63	0.02	0.43	0.41	0.653	0.125	0.191	0.112	1.050	10.16
67/1-P	3.59	0.53	1.47	0.62	0.00	0.03	0.64	0.02	0.41	0.39	0.662	0.136	0.205	0.156	1.149	10.27
68/1-P	3.56	0.56	1.46	0.67	0.00	0.04	0.64	0.01	0.44	0.42	0.669	0.134	0.200	0.170	1.040	10.26
70/1-P	3.60	0.47	1.52	0.62	0.00	0.03	0.66	0.01	0.40	0.39	0.710	0.132	0.186	0.095	1.112	10.27
75/1-P	3.43	0.61	1.57	0.69	0.00	0.03	0.61	0.02	0.57	0.43	0.612	0.154	0.252	0.222	1.345	9.99
79/1-P	3.48	0.62	1.51	0.67	0.00	0.05	0.58	0.01	0.52	0.42	0.603	0.112	0.186	0.188	1.777	9.89
81/1-P	3.54	0.57	1.48	0.67	0.00	0.03	0.63	0.01	0.46	0.42	0.711	0.100	0.141	0.150	1.234	10.15
47/1-I	3.50	0.71	1.33	0.78	0.00	0.05	0.53	0.01	0.50	0.50	0.450	0.075	0.167	0.350	2.468	9.95
49/1-I	3.54	0.58	1.44	0.72	0.00	0.03	0.60	0.01	0.46	0.46	0.550	0.098	0.178	0.311	1.867	10.14
51/1-I	3.57	0.64	1.38	0.68	0.00	0.03	0.59	0.02	0.43	0.43	0.519	0.086	0.166	0.299	2.110	10.20
69/1-I	3.55	0.62	1.42	0.67	0.00	0.04	0.58	0.01	0.45	0.42	0.486	0.088	0.181	0.308	1.850	10.10
71/1-I	3.57	0.56	1.45	0.68	0.00	0.03	0.61	0.01	0.43	0.43	0.558	0.099	0.177	0.260	1.500	10.20
78/1-I	3.50	0.73	1.33	0.76	0.00	0.05	0.52	0.01	0.50	0.49	0.368	0.073	0.199	0.343	2.468	9.86
90/1-I	3.47	0.65	1.46	0.74	0.00	0.04	0.56	0.01	0.53	0.46	0.380	0.083	0.218	0.305	2.210	10.02

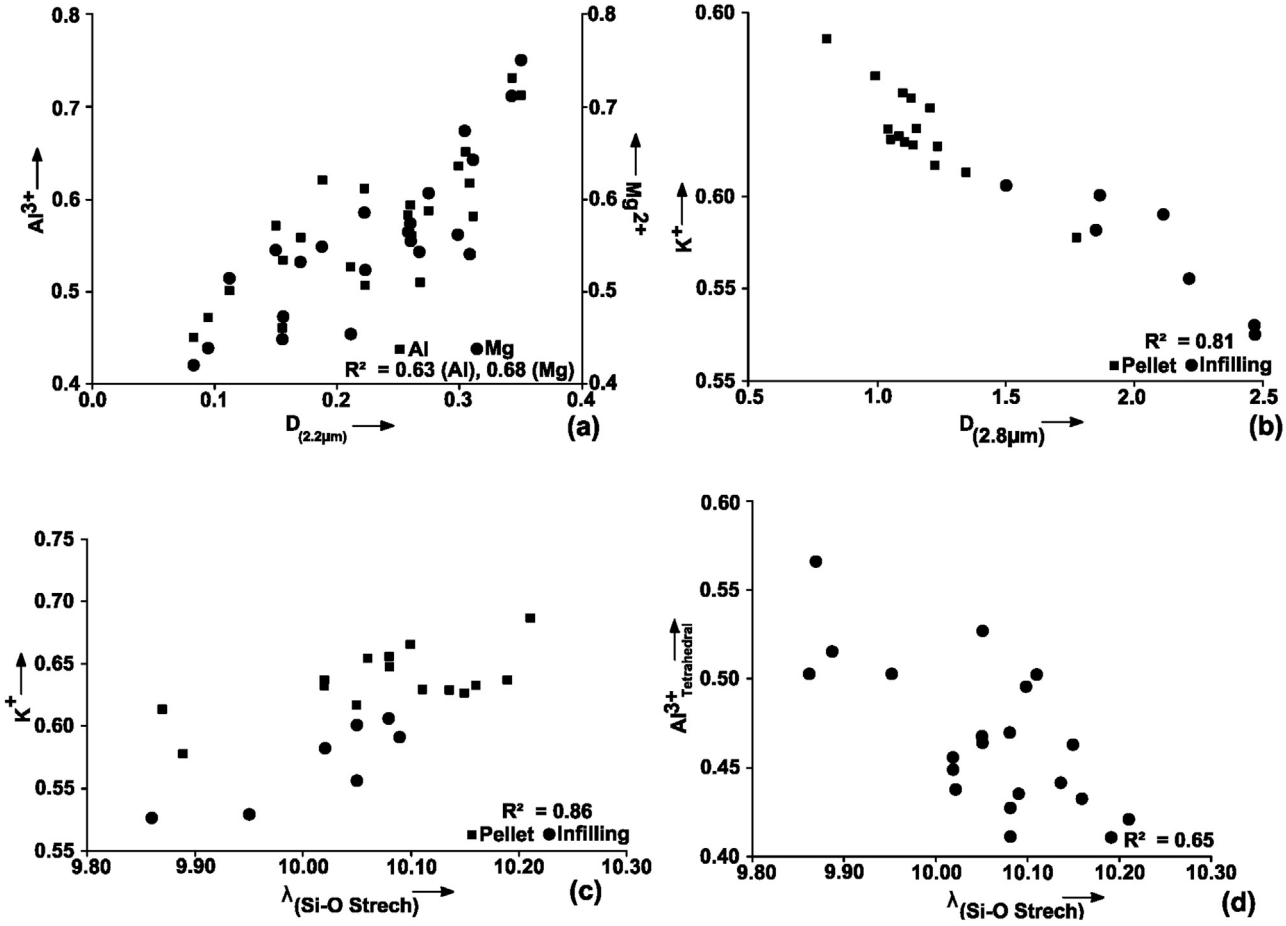

Fig. 5. Cross plots showing: (a) variation of cationic Mg^{2+} and Al^{3+} with the depth of the 2.2 μm absorption in reflectance spectra as a strong positive correlation; (b) depth of the 2.8 μm absorption vis-à-vis the K^+ content as a strong negative correlation indicating a decrease of Mg—OH bond influence with increasing maturity; (c) variation in wavelength of emissivity minima due to Si—O stretch with the K^+ content indicating a shift of band towards higher wavelengths with increasing maturity; and (d) variation in the wavelength of the absorbance minima due to the Si—O stretch with tetrahedral charge indicating decrease in tetrahedral charge with the shift of the band towards higher wavelengths.

$_{(Fe2+\text{-}Fe3+)CT}/D_{(Fe2+)dd}$ does not show any significant trend with increasing maturity indicating replacement of Fe^{2+} by Mg^{2+}. Both pellet and infilling spectra show weak absorption features at 1.395 and 1.415 μm caused by (OH—) overtone stretch and strong characteristic absorptions at 1.95–2.014 μm for the combination of H—O—H bend plus (OH—) stretch (Fig. 3). The simultaneous occurrence of both these absorptions indicates the occurrence of both (OH—) and H_2O in the mineral (Aines and Rossman, 1984; Clark, 1999). The stronger absorptions at 1.9–2 μm indicate the predominance of water over the hydroxyl ion (Fig. 3). Much of the H_2O relates to expandable smectite layers (Bailey, 1980; Deb and Fukuoka, 1998; Deer et al., 2013; Odin and Matter, 1981). Therefore, the less pronounced absorption at 1.9 μm band for pellets than infillings suggests low content of expandable layers.

A conspicuous absorption due to the combined influence of metal (Al, Mg)—OH bend plus OH stretch is noted near 2.2–2.3 μm in both infillings and pellets (Fig. 3). The absorption doublet is seen at the same location in the USGS spectra and corresponds to an (Al, Mg)—OH band (Fig. 3). This particular absorption is deeper for infillings but becomes weak in glauconitic pellets, with a tendency to form a single wide absorption band (Fig. 3). Both Mg^{2+} and Al^{3+} show a conspicuous negative trend with K^+ implying release of these two elements from the glauconite structure with maturity (Fig. 4c–d). Subsequent to this, a plot of Mg^{2+}-Al^{3+}-depth of the 2.2 μm absorption suggests an increase in depth of this absorption with increasing Al^{3+} and Mg^{2+} (Table 2, Fig. 5a). Therefore, the depth of the 2.2 μm absorption seems to be synchronized with the maturation process of glauconites.

5.2. Spectral signatures in the infrared spectrum

Spectral signatures of five representative samples reveal the existence of a prominent band at 2.8–2.9 μm (3400–3500 cm^{-1}) (Fig. 6). This relates to the stretching mode of OH^-, which is essential for glauconite and other clays. Emissivity spectra of selective pellets and infillings with varying K^+ content from 0.52 to 0.69 reveal a gradual decrease in band depth of the hydroxyl-stretching region from 2.47 in infillings to 1.32 in pellets (Fig. 6). The variation of the 2.8 μm band depth with K^+ content in all glauconite samples resembles the same trend (Fig. 5b). Another weak feature at 5.85–6.16 μm (1620 cm^{-1} band) is noted, which is associated with molecular H_2O (Fig. 6). More pronounced, sharp and symmetric features in emissivity spectra for infillings change to diffuse and become broad features in pellets. This indicates a decrease in expandable smectite layers as glauconites matures (Fig. 6). The weakest absorption band in the region at about 7.0 μm in some of the infilling spectra is caused by a carbonate phase that remained as impurities inherited in foraminiferaL shells (Fig. 6). The position of the 9–11 μm absorption changes with a continuous increase in the sharpness of the dip from infillings to pellets (Fig. 6). For the pellets, the emissivity minima varies from 9.87 to 10.21 μm (av. 10.07 μm). On the other hand, that of the infillings varies from 9.86

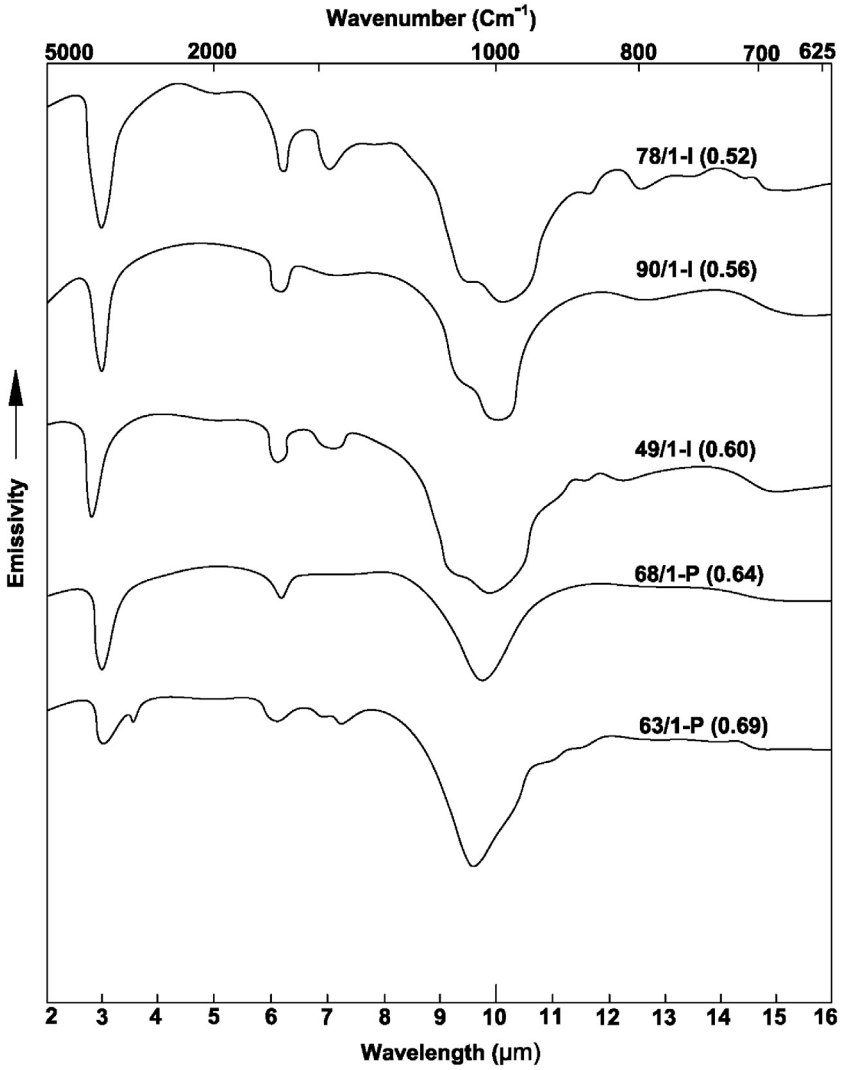

Fig. 6. Emissivity spectra of glauconite infillings and pellets in the 2–16 μm range showing a gradual decrease in the depth of the 2.8 μm band from infillings to pellets indicating the presence of less expandable smectitic layers in the later. A similar conspicuous shift in emissivity minima approximating 10 μm Si—O band, progressively, towards higher wavelengths is noted with an increase in K^+ content indicating diminishing expandable layers. (I and P in sample name column stand for glauconite infilling and pellet respectively with corresponding K^+ content in bracket) (Spectral offset given for clarity).

to 10.05 μm (av. 10.01) (Table 2, Fig. 6). This change of band position is correlated with the decreasing K^+ content (Fig. 5). A cross plot of the Si—O stretch minima vs K^+ reveals a shift of minima towards higher wavelengths with an increase in K^+ (Fig. 5c). The maturity of glauconite grains, i.e. decrease of expandable layers, is associated with a gradual shift of the Si—O vibration towards higher wavelengths (lower energy) (Fig. 5c). The cross plot of tetrahedral Al^{3+} of glauconites and band position of corresponding emissivity minima exhibits a moderate negative trend leading to an increase in band wavelength position with a decrease in tetrahedral Al^{3+} (Fig. 5d). The 10 μm absorption minima shifts towards lower wavelengths as Al^{3+} substitution increases in the tetrahedral site. The interlayer cationic content and tetrahedral Al^{3+} can be estimated by analyzing the shift of this absorption. The isomorphous substitution in the tetrahedral site is presumed to be the main causes of such shift.

The Maniyara Fort glauconite samples do not display an absorption near 7–7.5 μm, which is prominent in standard illite, Fe-smectite and montmorillonite. The most prominent band for glauconite is reported close to 10 μm. Representative spectra of infillings and pellets exhibit similar emissivity minima close to 10 μm.

6. Discussion

Evolved glauconite with high-K content is an indicator of a slow rate of sedimentation, therefore, it is considered as a crucial component of high-resolution sequence stratigraphic interpretations for a sedimentary basin (Amorosi, 1995). Besides, evolved glauconite is a valuable datable mineral in argillaceous rocks (Stille and Clauer, 1994). Evolved glauconite is also used as an important source of alternate potash fertilizer (Franzosi et al., 2014). Spectroscopic characterization of evolved glauconites is, therefore, significant for both academia and industry. Although EPMA and X-ray diffraction parameters can precisely estimate the K content of glauconite, the spectral characterization of glauconite holds promise as an alternate method which is fast, non-invasive and inexpensive.

The spectral response of the Maniyara Fort glauconites in the VIS-NIR range are found to be unique. The Fe^{2+} content in glauconite is within 10–15% of total iron (Bailey, 1980; Odin and Matter, 1981; Odom, 1984). In the visible range, Fe^{2+} generates a dd transition band. An advance oxidation process also gives rise to the development of a Fe^{2+}-Fe^{3+} charge transfer (CT) band in their reflectance spectra (Amthauer and Rossman, 1984; Rossman, 1988a,b). The lesser depth of absorption for glauconite infillings than that of the

pellet is a proxy of their maturity state. The absorption band asymmetry factor (see van der Meer, 2004) is observed to be slightly higher in the case of infillings than pellets. The metal–metal charge-transfer (CT) is common in other mica group of minerals (Bishop et al., 2008; Robbins and Strens, 1972). However, the present work differentiated glauconites with different modes of origin. Less Fe^{2+} substantially affects the ratio between intensities of absorption due to (Fe^{2+}-Fe^{3+}) CT and (Fe^{2+}) dd resulting in the lack of a correlation with K^+. High Mg^{2+} in the octahedral site solicits intense replacement of Fe^{2+} in the octahedral site of glauconite giving rise to low Fe^{2+} (Table 2). These results demonstrate the importance of an isomorphic cationic substitution on spectral absorptions.

Sanchez-Navas et al. (2008) attempted to relate the ratio of dd transition and CT absorptions with the colour of glauconites. However, the Siberian glauconite reported by Sanchez-Navas et al. (2008), is less matured, although rich in Fe. In the Maniyara Fort Formation, the iron content of glauconites, however, increases with increased maturity (Banerjee et al., 2012b).

Burst (1958a,b) reported that most glauconites belong to the "inter-layered" class, involving interlayering between montmorillonite-type (expandable) and illite-type (non-expandable) layers (Hower, 1961; Manghnani and Hower, 1964a,b). Differential water content in glauconites is related to the presence of expandable layers in glauconites (Figs. 3 and 6). The spectral signature of glauconite is also important for estimation of its maturation. The Si—O stretching vibration causes maximum absorption between 9 and 11 μm. The same absorption in the case of micas is influenced by Y-number or the amount of Al^{3+} substituted for Si^{4+} in the tetrahedral site (Lyon and Tuddenham, 1960; Milkey, 1960). The Y number has subsequently been renamed as the tetrahedral charge (Bailey, 1980; Odom, 1984). An interrelation between tetrahedral charge, K_20 content and emissivity minima has revealed similar features for the studied glauconite.

7. Conclusions

The study of the spectral response of the Maniyara Fort glauconites leads to the following conclusions.

a. In the VIS-NIR region, a metal–metal CT absorption at 0.77 μm and a Fe^{2+}dd absorption at 1.08 μm correlate positively with K^+ and $Fe_2O_{3(total)}$. A thorough replacement of Fe^{2+} by Mg^{2+} within the octahedral site of glauconite results in a weak correlation between glauconite maturity and $D_{(Fe^{2+}\text{-}Fe^{3+})CT}/D_{(Fe^{2+})dd}$ ratio.
b. The relatively weaker absorption depth at 2.3 μm in the spectra of pellets compared to infillings indicates a moderate negative correlation between Mg^{2+} and K^+. Therefore, the absorption depth may be used to estimate the amount of octahedral Mg^{2+} content in glauconites.
c. H_2O and OH^- signatures at 1.9 μm and 2.8–2.9 μm suggest the association (or presence) of molecular H_2O with expandable smectites in the interlayered glauconite structure. Because of their lesser content of expandable layers and greater maturation, pellets exhibit a less pronounced depth in reflectance and emissivity spectra compared to infilling.
d. An increase in K_2O content results in a gradual shift of the 10 μm emissivity minima toward higher wavelengths, which is related to the Si—O stretch. The shift estimates the tetrahedral charge in glauconites as well, which is related to the ionic substitution between Si^{4+}-Al^{3+}.

Acknowledgements

SLC and SB are thankful to the Department of Science and Technology, Government of India for financial support (grant no. AR/S4/ES-281/2007). SLC and PKC acknowledge infrastructural support provided by the Indian Institute of Remote Sensing, Dehradun. Help received from Mrs. Richa Sharma, Mr. Vivek Sengar and Mr. Gokul in collection of spectra using the ASD and FTIR in the hyperspectral lab of IIRS, Dehradun are also duly acknowledged. Authors are also thankful to the anonymous reviewer whose inputs substantially enhanced the quality of the earlier versions of draft.

References

Aines, R.D., Rossman, G.R., 1984. Water in minerals? A peak in the infrared. J. Geophys. Res. 89 (B6), 4059–4071.
Amorosi, A., Sammartino, I., Tateo, F., 2007. Evolution patterns of glaucony maturity: a mineralogical and geochemical approach. Deep-Sea Res. Part II: Top. Stud. Oceanogr. 54, 1364–1374.
Amorosi, A., 1995. Glaucony and sequence stratigraphy: a conceptual framework of distribution in siliciclastic sequences. J. Sediment. Res. B 65, 419–425.
Amorosi, A., 1997. Detecting compositional, spatial, and temporal attributes of glaucony: a tool for provenance research. Sediment. Geol. 109, 135–153.
Amthauer, G., Rossman, G.R., 1984. Mixed valence of iron in minerals with cation clusters. Phys. Chem. Miner. 11, 37–51.
Archer, S., Gartley, M., Kerekes, J., Cosofret, B., Giblin, J., 2015. Empirical measurement and model validation of infrared spectra of contaminated surfaces. In: Velez-Reyes, M., Kruse, F.A. (Eds.), Proceedings, SPIE Algorithms and Technologies for Multispectral, Hyperspectral, and Ultraspectral Imagery XXI, SPIE, vol. 9472., http://dx.doi.org/10.1117/12.2177683 (947215-1).
Bailey, S.W., 1980. Summary of recommendations of AIPEA nomenclature committee 328 on clay minerals. Clays Clay Miner. 28, 73–78.
Banerjee, S., Chattoraj, S., Saraswati, P.K., Dasgupta, S., Sarkar, U., Bumby, A., 2012a. The origin and maturation of lagoonal glauconites: a case study from the Oligocene Maniyara Fort Formation, western Kutch, India. Geol. J. 47, 357–371.
Banerjee, S., Chattoraj, S., Saraswati, P.K., Dasgupta, S., Sarkar, U., 2012b. Substrate control on formation and maturation of glauconites in the Middle Eocene Harudi Formation western Kutch, India. Mar. Petrol. Geol. 30, 144–160.
Banerjee, S., Mondal, S., Chakraborty, P.P., Meena, S.S., 2015. Distinctive compositional characteristics and evolutionary trend of Precambrian glaucony: example from Bhalukona Formation Chhattisgarh basin, India. Precam. Res. 271, 33–48.
Banerjee, S., Bansal, U., Pande, K., Meena, S.S., 2016a. Compositional variability of glauconites within the Upper Cretaceous Karai Shale Formation, Cauvery Basin, India: implications for evaluation of stratigraphic condensation. Sediment. Geol. 331, 12–29.
Banerjee, S., Bansal, U., Thorat, A., 2016b. A review on palaeogeographic implications and temporal variation in glaucony composition. J. Palaeogeogr. 5, 43–71, http://dx.doi.org/10.1016/j.jop.2015.12.001.
Besson, G., Drits, V.A., 1997. Refined relationships between chemical composition of dioctahedral fine-grained mica minerals and their infrared spectra within the OH stretching region, part-I: identification of the OH stretching bands. Clays Clay Miner. 45 (2), 158–169.
Bishop, J., Madejovâ, J., Komadel, P., Froschl, H., 2002. The influence of structural Fe, Al and Mg on the infrared OH bands in spectra of dioctahedral smectites. Clay Miner. 37, 607–616.
Bishop, J.L., Lane, M.D., Dyar, M.D., Brown, A.J., 2008. Reflectance and emission spectroscopy study of four groups of phyllosilicates: smectites, kaolinite, serpentines, chlorites and micas. Clay Miner. 43, 35–54.
Biswas, S.K., 1992. Tertiary stratigraphy of kutch. J. Palaeontol. Soc. Ind. 37, 1–29.
Buckley, B., Bevan, I.C., Brown, K.M., Jonson, L.R., Farmer, V.C., 1978. Glauconites and celadonites: two separate mineral species. Mineral. Mag. 42, 373–382.
Burns, R., 1993. Mineralogical Applications of Crystal Field Theory, second ed. Cambridge University Press, Cambridge.
Burst, J.F., 1958a. 'Glauconite' pellets: their mineral nature and applications to stratigraphic interpretations. Am. Assoc. Pet. Geol. Bull. 42, 310–327.
Burst, J.F., 1958b. Mineral heterogeneity in 'Glauconite' pellets. Am. Mineral. 43, 481–497.
Chattoraj, S., Banerjee, S., Saraswati, P.K., 2008a. Sedimentation, palaeogeography and sequence stratigraphic framework of late palaeocene to early eocene naredi formation, western kutch, Gujarat. Int. Assoc. Gond. Res. Conf. Ser. 5 (p.116).
Chattoraj, S.L., Banerjee, S., Saraswati, P.K., 2008b. Glauconitic minerals from green shales late paleocene to early eocene naredi formation, western kutch, gujarat. In: 25th Annu. Convention Indian Assoc. Sedimentol., Baroda, 26th–28th December (p. 35).
Chattoraj, S.L., Banerjee, S., Saraswati, P.K., 2009. Glauconites from the late palaeocene-early eocene naredi formation, western kutch and their genetic implications. J. Geol. Soc. India 73, 567–574.
Chattoraj, S.L., 2011. Glauconite Formation in Stratigraphic Framework of Palaeogene Succession in Kutch Unpublished Ph.D. Thesis. Indian Institute of Technology Bombay, Mumbai, India (p. 241).
Chattoraj, S.L., 2016. Glauconite in Stratigraphic Framework of Palaeogene of Kutch, India. Lambert Academic Publishing, Saarbrücken, Germany (ISBN: 978-3-659-97455-7).

Clark, R.N., King, T.V.V., Gorelick, N.S., 1987. Automatic continuum analysis of reflectance spectra. In: Proc. Third AIS Workshop (2–4 June, 1987), JPL Publication 87–30. Jet Propulsion Laboratory, Pasadena, California, pp. 138–142.
Clark, R.N., King, T.V.V., Klejwa, M., Swayze, G.A., 1990. High spectral resolution spectroscopy of minerals. J. Geophys. Res. 95 (B8), 12653–12680.
Clark, R.N., 1983. Spectral properties of mixtures of montmorillonite and dark carbon grains: implications for remote sensing minerals containing chemically and physically adsorbed water. J. Geophys. Res. 88, 10635–10644.
Clark, R.N., 1999. Spectroscopy of rocks and minerals. In: Rencz, A.N. (Ed.), Manual of Remote Sensing, Remote Sensing for the Earth Sciences, Spectroscopy of Rocks and Minerals and Principles of Spectroscopy, vol. 3. John Wiley and Sons, New York, pp. 3–58.
Crowley, J.K., Vergo, N., 1988. Near-infrared reflectance spectra of mixtures of kaolin group minerals: use in clay studies. Clays Clay Miner. 36, 310–316.
Deb, S.P., Fukuoka, M., 1998. Fe-illites in a Proterozoic deep marine slope deposit in the Penganga Group of the Pranhita Godavari valley-their origin and environmental significance. J. Geol. 106, 741–749.
Deer, W.A., Howie, R.A., Zussman, J., 2013. An Introduction to the Rock-forming Minerals. Longman, London, pp. 193–340.
Franzosi, C., Castro, L.N., Celeda, A.M., 2014. Technical evaluation of glauconites as alternative potassium fertilizer from the salamanca formation, patagonia, southwest Argentina. Nat. Res. Res. 23 (3), http://dx.doi.org/10.1007/s11053-014-9232-1.
Green, A.A., Craig, M.D., 1985. Analysis of aircraft spectrometer data with logarithmic residuals. In: Proc. AIS Workshop, (8–10 April, 1985), JPL Publication 85–41. Jet Propulsion Laboratory, Pasadena, California, pp. 111–119.
Hower, J., 1961. Some factors concerning the nature and origin of glauconite. Am. Miner. 46, 313–334.
Hunt, J.M., Turner, D.C., 1953. Determination of mineral constituents of rocks by infrared spectroscopy. Anal. Chem. 25, 1169–1174.
Jarrar, G., Amireh, B., Zachmann, D., 2000. The major, trace and rare earth element geochemistry of glauconites from the early Cretaceous Kurnub Group of Jordan. Geochem. J. 34, 207–222.
Kruse, F.A., Raines, G.L., Watson, K., 1985. Analytical techniques for extracting geologic information from multichannel airborne spectroradiometer and airborne imaging spectrometer data. In: Proc. Int. Symp. Remote Sens. of Envt, Fourth Thematic Conf Remote Sensing for Exploration Geology, San Francisco, California (1–4 April, 1985), pp. 309–332.
Lyon, R.J.P., Tuddenham, W.M., 1960. Determination of tetrahedral aluminum in mica by infrared absorption analysis. Nature 185, 374–375.
Manghnani, M.H., Hower, J., 1964a. Glauconites: cation exchange capacities and infrared spectra. Part I: the cation exchange capacity of glauconite. Am. Miner. 49, 586–598.
Manghnani, M.H., Hower, J., 1964b. Glauconites: cation exchange capacities and infrared spectra. Part II: infrared absorption characteristics of glauconites. Am. Miner. 49, 1631–1642.
Milkey, R.G., 1960. Infrared spectra of some tectosilicates. Am. Miner. 45, 990–1007.
Mitra, S., 1996. Fundamentals of Optical, Spectroscopic and X-ray Mineralogy. New Age International Publishers, New Delhi, India (p. 336).
Nahin, P.G., 1955. Infrared analysis of clay and related minerals. Clays Clay Technol. Bull. 169, 112–118.
Odin, G.S., Fullagar, P.D., 1988. Geological significance of the glaucony facies. In: Odin, G.S. (Ed.), Green Marine Clays. Elsevier, Amsterdam, pp. 295–332.
Odin, G.S., Matter, A., 1981. De glauconiarum origine. Sediment 28, 611–641.
Odom, E.I., 1984. Glauconite and celadonite minerals. in: Bailey, S.W. (Ed.), Micas. Rev. Mineral. 13, 545–584.
Petit, S., Righi, D., Madejova, J., Decarreau, A., 1998. Layer charge estimation of smectites infrared spectroscopy. Clay Miner. 33, 579–591.
Petit, S., Madejovaí, J., Decarreau, A., Martin, F., 1999. Characterization of octahedral substitutions in kaolinites using near-infrared spectroscopy. Clays Clay Miner. 47, 103–108.
Post, J.L., Noble, P.N., 1993. The near-infrared combination band frequencies of dioctahedral smectites, micas, and illites. Clays Clay Miner. 41, 639–644.
Raju, D.S.N., 1974. Study on indian miogypsinidae. Utrecht Micropalaeontol. Bull. 9, 1–148.
Robbins, D.W., Strens, R.G.J., 1972. Charge-transfer in ferromagnesian silicates: the polarized electronic spectra of trioctahedral micas. Mineral. Mag. 38, 551–563.
Rossman, G.R., 1988. Optical Spectroscopy. in: Hawthorne, F.C. (Ed.), Spectroscopic Methods in Mineralogy and Geology. Rev. Miner. 18, 207–254.
Rossman, G.R., 1988. Vibrational Spectroscopy of Hydrous Components. in: Hawthorne, F.C. (Ed.), Spectroscopic Methods in Mineralogy and Geology. Rev. Miner. 18, 193–206.
Salvaggio, C., Miller, C.J., 2001. Methodologies and protocols for the collection of midwave and longwave infrared emissivity spectra using a portable field spectrometer. Orlando, Florida, USA In: Proc. SPIE, SPIE, AeroSense, Image Exploitation and Target Recognition, Algorithms and Technologies for Multispectral, Hyperspectral, and Ultraspectral Imagery VII, vol. 4381, pp. 539–548.
Sanchez-Navas, A., Martín-Algarra, A., Eder, V., Reddy, B.J., Nieto, F., Zanin, Y.N., 2008. Color, mineralogy and composition of upper Jurassic west Siberian glauconite: useful indicators of paleoenvironment. Can. Miner. 46, 1545–1564.
Saraswati, P.K., 1995. Biometry of early oligocene lepidocyclina from Kutch, India. Mar. Micropaleontol. 26, 303–311.
Singh, I.B., 1978. Microfacies, petrography and mineralogy of the Tertiary rocks of Guar Nala near Narayan Sarovar, Kutch, India, and their palaecological significance. J. Palaeontol. Soc. India 21–22, 78–95.
Slonimskaya, M.V., Besson, G., Dainyak, L., Tchoubar, G.C., Drits, V.A., 1986. Interpretation of the IR spectra of celadonites and glauconites in the region of OH-stretching frequencies. Clay Miner. 21, 377–388.
Stille, P., Clauer, N., 1994. The process of gluconitization: chemical and isotopic evidence. Contrib. Miner. Petrol. 117, 253–262.
Yamaguchi, Y., Lyon, R.J.P., 1986. Identification of clay minerals by feature coding of near-infrared spectra. Proc. Int. Symp. Remote Sens. Env., First Thematic Conf. for Remote Sensing for Exploration Geology, ERIM, 627–636.
van der Meer, F.D., 2004. Analysis of spectral absorption features in hyperspectral imagery. Int. J. Appl. Earth Obs. Geoinf. 5, 55–68.